Published in final edited form as:

Nat Biomed Eng. 2019 December ; 3(12): 998–1008. doi:10.1038/s41551-019-0458-4.

Aberrant mechanosensing in injured intervertebral discs as a result of boundary-constraint disruption and residual-strain loss

Edward D. Bonnevie[1,2], **Sarah E. Gullbrand**[1,2], **Beth G. Ashinsky**[2,3], **Tonia K. Tsinman**[1,2], **Dawn M. Elliott**[4], **Pen-hsiu Grace Chao**[5], **Harvey E. Smith**[1,2], **Robert L. Mauck**[1,2,*]

[1]University of Pennsylvania, 36th St and Hamilton Walk, Philadelphia, PA 19104

[2]CMC VA Medical Centre, 3900 Woodland Ave, Philadelphia, PA 19104

[3]Drexel University, 3141 Chestnut St, Philadelphia, PA 19104

[4]University of Delaware, 150 Academy Street, Newark, DE 19716

[5]National Taiwan University, No. 1, Section 4, Roosevelt Rd, Da'an District, Taipei City, Taiwan 10617

Abstract

In fibrous tissues, pre-stressed boundary constraints at bone interfaces instil residual strain throughout the tissue, even when unloaded. For example, internal swelling pressures in the central nucleus pulposus of the intervertebral disc generate pre-strain in the outer annulus fibrosus. With injury and depressurization, these residual strains are lost. Here, we show that the loss of residual strains in the intervertebral disc alters the microenvironment and instigates aberrant tissue remodelling and the adoption of atypical cellular phenotypes. By using puncture surgery of the annulus fibrosus in rabbits, ex vivo puncture experiments, and electrospun nanofibrous scaffolds recapitulating evolving boundary constraints, we show that the loss of residual strain promotes short-term apoptosis and the emergence of a fibrotic phenotype, that local fibre organization and cellular contractility mediate this process, and that the aberrant cellular changes could be abrogated by targeting the cell-mechanosensing machinery with small molecules. Our findings

*Correspondence and requests for materials should be addressed to Robert Mauck lemauck@pennmedicine.upenn.edu.

Author contributions

Conceived and designed the experiments: EDB, HES, DEM, RLM
Performed the experiments: EDB, SEG, BGA, TKT, PGC, HES
Analyzed the data: EDB, SEG, BGA
Contributed materials/analysis tools: TKT, PGC
Manuscript writing: EDB, RLM
Manuscript editing: EDB, SEG, BGA, TKT, DEM, PGC, HES, RLM

Reporting summary. Further information on research design is available in the Nature Research Reporting Summary linked to this article.

Data availability

The main data supporting the results in this study are available within the paper and its Supplementary Information. The raw and analysed datasets generated during the study are available for research purposes from the corresponding authors on reasonable request.

Competing interests

The authors declare no competing interests.

indicate that injury to dense connective tissues under pre-strain alters boundary constraints and residual strain, leading to aberrant mechanosensing, which in turn promotes disease progression.

Injury and degeneration of the intervertebral discs, the soft tissue segments of the spine, is associated with debilitating back pain and loss of mobility[1, 2]. Despite the large financial burden associated with back pain, the processes following disc injury that culminate in full-scale degeneration are not well understood. Further, understanding these processes is difficult to achieve given the complex mechanical environments associated with both healthy and diseased states[3-5]. In healthy discs, an inner, gel-like region (nucleus pulposus, NP) maintains a high osmotic swelling pressure (on the order of 100 kPa) that engages with and is confined by a peripheral ligament-like annulus fibrosus (AF), which also serves to mechanically connect adjacent vertebrae[6,7]. Under static equilibrium, the swelling pressure in the NP creates residual strains (pre-strains) in the AF that exceed ε=10% in the outer region[8]. Hallmarks of disc injury and degeneration include a loss of swelling pressure and herniation of NP material through a compromised AF. Thus, a contributing factor in disc degeneration is the release of residual strains in the AF due to severed fiber connectivity and a loss of NP pressure. We hypothesize that this altered boundary constraint modulates the mechanical environment of the cells within the AF, initiating subsequent fibrotic remodeling.

In both healthy and diseased states, cells within tissues utilize their contractile machinery to probe and surveil the local microenvironment[9]. Cues such as stiffness and topography direct downstream mechanically-active signaling that ultimately regulates cell function and fate[10,11]. It has becoming increasingly well understood that a suite of mechano-sensitive factors (e.g., YAP/TAZ, MRTF-A) relay these local mechanical cues to the nucleus and tune cellular homeostasis[10,12]. In the context of disc degeneration, the AF undergoes mechanical, biochemical, and organizational changes[13]. These changes occur in parallel with a loss of swelling in the NP, leading to a loss of the residual strains in the AF. It is currently unknown how this altered mechanical and topographical state is sensed by the resident, fibroblast-like cells in the AF, and whether and how this evolving environment directs the aberrant remodeling that culminates in disc degeneration.

Here, we test the hypothesis that a change in residual strain (i.e., rapid loss of a pre-strained boundary constraint) in an otherwise organized fiber environment provides emergent biophysical cues to AF cells that promote their transition to a fibrotic phenotype. To test this hypothesis, we utilized an established puncture model in the rabbit that severs AF connectivity and releases residual strains relative to the healthy disc environment[14]. In this model, we assessed the time evolution of disc mechanics, AF fiber re/organization, and phenotypic changes in the AF region of the degenerating disc. To separate the specific inputs arising from changing boundary constraints from other factors present in a wound environment, we developed a scaffold system (based on electrospun scaffolds) in which both the level of fiber organization and/or fiber pre-strain could decoupled to assess AF cell response to organization and time-evolving boundary constraints. Finally, using this scaffold system, we show that pharmacologic agents targeting cellular contractility can interrupt the

activation of aberrant mechano-transductive events with a loss of prestrain that ultimately leads to disc degeneration.

Release of Residual Strain Leads to an Aberrant, Fibrotic Phenotype in the Annulus Fibrosus

To assess how releasing residual strains translates to progressive disc degeneration, we performed annular puncture[14] in the lumbar discs of New Zealand White rabbits (Fig 1a) with survival to 2, 4, and 8 weeks. Following sacrifice, we assessed bulk mechanical properties to determine the low strain (i.e., toe-region or neutral zone) modulus and range of motion (SFig 1)[15]. After 2 weeks, range of motion increased, corresponding with a decrease in toe modulus (Fig 1bc). At 4- and 8-weeks, as degeneration progressed, the range of motion decreased, corresponding to an increase in modulus. To determine the origin of these mechanical changes, we assessed the fiber organization of the AF via second harmonic generation (SHG) imaging and determined the fiber angle distribution using fast Fourier transform. Angular spread[16] was calculated as the standard deviation of a Gaussian fit to the fiber angle distribution (SFig 2). With time post injury, the AF became progressively disorganized, with the angular spread reaching levels > 80° at 8 weeks (Fig 1d,f-i). This progressive stiffening of the disc and increased disorganization are consistent with fibrotic remodeling[17], and so we next assessed AF cell phenotype after injury. After disc injury and loss of prestrain, AF cells showed higher levels of alpha smooth muscle actin (αSMA) at 2 weeks, which remained elevated through 8 weeks (Fig 1e,j-m, SFig 3). In most wound environments, emergence of αSMA indicates the development of a highly contractile, myofibroblast-like phenotype[17,18].

Prestrain in Engineered Fibrous Environments Dictates Mechanobiologic Cues

While intriguing, this *in vivo* injury model involves multiple factors that change simultaneously, making it difficult to decouple pre-strain mediated effects from those present in the wound environment. To that end, we next developed a biomaterial culture system to evaluate how altered boundary constraints and fiber organization might drive changes in cellular behavior. This system was designed to mimic the boundary constraints (i.e., the residual strains) and the fiber topography observed with progressive degeneration in the animal model. For this, electrospun poly(ε-caprolactone) nanofibrous scaffolds (SFig 4) were formed as aligned or disorganized templates[19] and were clamped in a tensile culture device actuated by a lead screw (Fig 2a) that allowed strain to be applied to the network prior to cell seeding (Fig 2b). Mounting this device in an environmental scanning electron microscope (ESEM) enabled comparison of fiber organization between the native degenerating AF (Fig 1d, SFig 2) and scaffolds (Fig 2cd, SFig 5). Both aligned and non-aligned scaffolds showed increased organization (i.e., decreased angular spread) as a function of applied strain, which plateaued at ~ 9%, consistent with the toe-region of the scaffold mechanics (SFig 5). These scaffolds were then seeded with AF cells in the presence or absence of prestrain (by stretching the scaffolds prior to cell seeding, Fig 2b). Scaffold alignment (aligned versus nonaligned) directed cell and nuclear orientation (SFig 5), with

prestrain of aligned scaffolds significantly increasing cell and nuclear aspect ratio relative to other groups (Fig 2def).

Given that prestrain of the aligned scaffold group increased cell elongation upon seeding, we next asked whether this prestrained, organized topography impacted cellular sensation of the local fibrous environment by measuring nuclear localization of the transcriptional co-activators YAP/TAZ[10,20,21]. In 2D, YAP/TAZ translocates to the nucleus in cells on stiff environments, a phenomenon that is conserved for AF cells (SFig 6). In the context of our fiber environments, however, we found that YAP/TAZ localization depended on prestrain and organization in a counter-intuitive manner. Specifically, despite seeding AF cells onto strain-stiffened (SFig 5), aligned scaffolds nuclear levels of YAP/TAZ were reduced compared to all other groups (Fig 2g). To establish whether this mechanobiologic response was unique to YAP/TAZ, we also assessed focal adhesion formation[9]. Staining for paxillin revealed a similar trend, where total focal adhesion area per cell was lower in aligned, prestrained scaffolds compared to other groups (Fig 2kl). On a cell-by-cell basis, across the range of microenvironments presented to AF cells, there were significant trends of decreased nuclear YAP/TAZ with increased cell aspect ratio ($r = -0.26$, $p = 0.0002$) and increased nuclear aspect ratio ($r = -0.2$, $p = 0.004$), and increased nuclear YAP/TAZ with increased cell spread area ($r = 0.44$, $p < 0.00001$), while other shape factors such as circularity and solidity did not provide significant correlations (SFig 7). These findings suggested that prestrain-driven fiber organization altered the fibrous template to regulate cell shape and size, which in turn, dictated cellular sensation of the local environment. To determine if this was the case, we utilized micro contact printing of 2D substrates to control cell spreading and aspect ratio. On narrow patterns (15 μm stripes), increased cell aspect ratio and nuclear aspect ratio, and decreased nuclear YAP/TAZ were observed (SFig 8). Together, these data support the hypothesis that topographical features that promote AF cell elongation in a single direction (1D) limit YAP/TAZ nuclear entry, regardless of the stiffness of the substrate.

Since modulating cell shape and size can alter mechanosensation, we next sought to understand how boundary condition-mediated changes in local fiber topography dictates interpretation of such cues by resident cells. We quantified the angular spread of the fibrous network local to cells and compared this metric to shape parameters, focal adhesion area, and YAP/TAZ nuclear localization. This analysis, on a cell-by-cell basis, and across the range of scaffold conditions, revealed a spectrum of local fiber organizations (Fig 3ab) that corresponded well with the ESEM analysis (Fig 2, SFig 5). Moreover, this variation in local fiber organization predicted cell shape parameters (Fig 3cd), with micro-scale regions of higher organization showing increased cellular aspect ratio ($r = -0.61$, $p < 0.00001$, Fig 3c) and decreased cell spread area ($r = 0.52$, $p < 0.00001$, Fig 3d). Focal adhesion area was also predicted by local fiber organization, with organized fiber micro-scale regions curtailing focal adhesion growth ($r = 0.45$, $p = 0.0003$, Fig 3ef), resulting in lower nuclear YAP/TAZ ($r = 0.62$, $p = 0.00002$, Fig 3gh). Together, these data suggest that prestrain-mediated fiber alignment increases the likelihood that a cell will encounter a highly aligned micro-scale region within the scaffold, resulting in increased elongation and reduced focal adhesion area, and subsequent retention of YAP/TAZ in the cytosol.

In the *in vivo* scenario, puncture resulted in loss of prestrain and a decrease in fiber organization, and this corresponded with the emergence of fibrotic phenotypes (Fig 1). To determine whether the scaffold system would recapitulate this phenomenon, AF cells were assessed for fibrotic markers. Consistent with other contractile cell types[12,18], AF cells adopt an αSMA+ phenotype with increasing 2D substrate stiffness (SFig 6). Conversely, on fiber networks, αSMA incorporation into stress fibers increased in the absence of prestrain and with increasing disorder (Fig 4ab). As this emergent fibrotic phenotype is often associated with mechanosensing on stiff matrices, we queried whether this phenotype could be attenuated with small molecule therapeutics targeting cell mechanosensing. With application of the ROCK inhibitor Fasudil (used clinically to treat cerebral vasospasm), the transition to an SMA+ phenotype on glass substrates (SFig 9a) was attenuated, in line with a decrease in nuclear levels of YAP/TAZ (SFig 9b). Additionally, blocking YAP/TAZ binding to TEAD directly with verteporfin (a drug used clinically to treat macular degeneration) abrogated the fibrotic phenotype on glass substrates as well, and decreased cell spreading in a dose-dependent manner (SFig 9c). Taken together, these findings support that activation of mechanosensing, through the YAP/TAZ pathway, can instigate fibrotic remodeling in AF cells.

Given that the myofibroblast-like phenotype is associated with excessive matrix deposition and fibrotic remodeling in vivo (Fig 1)[17], we assessed nascent matrix deposition on a single-cell basis in the context of the local fiber environment. Functional non-canonical amino acid tagging (FUNCAT[22,23]) with a methionine analog (L-Azidohomoalanine, AHA) showed that the area of nascent matrix deposition (SFig 10, r = 0.50, Fig 4cd) increased with increased mechano-signaling in disorganized fibrous networks. These findings support the hypothesis that emergent disorder modulates contractility-dependent mechanosensing to promote fibrotic remodeling, in a manner dictated not by local stiffness, but rather by tension-mediated (re)organization of the fiber network.

Release of Residual Strain Acutely Alters the Fiber Environment and Triggers Cellular Responses

While the above findings indicate that the long-term effects of releasing residual strains alter the fiber environment and cellular phenotype, it is unclear how cells respond acutely to such evolving boundary constraints (e.g., the acute unloading of a fiber environment in injury). To evaluate the acute effects of severing AF connectivity, we mounted motion segments (i.e., vertebra-disc-vertebra) from the lumbar spine of rabbits beneath the objective of a multiphoton microscope to visualize changes to fibrous topography occurring immediately after the puncture injury (Fig 5a). Second harmonic generation (SHG) imaging of collagen revealed considerable changes to the fibrous AF following puncture (Fig 5b). At the level of the motion segment, the bulk mechanics of the disc were immediately transformed, with tension-compression testing[15] showing a decreased toe region modulus and increased toe range of motion (Fig 5de, SFig 1). These data indicate that severing AF connectivity releases the residual strains imbued in the healthy AF, and that this injury perturbs the overall function of the disc, where NP pressurization translates to tensile hoop stresses in the AF[24].

To determine whether AF cells respond biologically to this release of residual strain, explanted motion segments (L2/L3 and L3/L4) were subjected to needle puncture and then cultured for 24 hours. Immunofluorescence coupled with SHG revealed altered fiber morphology, change in cell shape, and increased levels of active caspase 3 in the vicinity of the puncture (Fig 4ef, SFig 11). This emergent apoptotic process is consistent with recent reports of cell death in other fibrous tissues, such as tendon, that have been subjected to complete transection[25,26]. However, it is unknown how such injuries that cause immediate changes to the fiber environment lead to aberrant cellular responses.

Release of Prestrain Re-Initiates Cellular Surveillance and Triggers Apoptosis

To begin to decouple the complex environmental changes in disc injury, we again utilized our biomaterial system, where acute responses of cells to altered boundary constraints could be evaluated in the absence of confounding factors. Cells were seeded onto aligned, prestrained scaffolds (4% or 9% strain) and either stretched (4%→9%) or released (9%→4%) (Fig 6a). While we and others have shown that cells respond to acute stretch[27], the disc puncture model results in acute unloading of the fiber environment. To address this, we used this system to evaluate how cell response to unloading (release of prestrain) differs from cell response to loading (stretch) in a fibrous microenvironment. After 24 hours of preculture, strain transfer from the boundaries through the scaffold and to the cells was assessed by changes in the nuclear aspect ratio[20]. Both stretch and release resulted in strain transfer to cells, with nuclear aspect ratios changing by >3% following a 5% change in strain, in both stretch and release configurations (Fig 6b, SFig 12). Following both stretch and release, spontaneous calcium signaling was monitored to assess altered homeostasis and re-initiation of cellular surveillance (Fig 6cd, SFig 13)[27-29]. As has been previously reported[27,28], the percent of cells responding following stretch significantly increased (Fig 6e). Interestingly, release of strain also significantly increased the proportion of cells responding, and did so by a similar magnitude (Fig 6e). This indicates that both loading and unloading elicit a mechano-response. Despite these similarities, 24 hours following stretch or release, a differential response was observed with respect to apoptosis (Fig 6f-j). Specifically, release of strain significantly increased the proportion of active caspase 3 positive cells, while the same magnitude of additional stretch did not. It should be noted that the acute change in boundary constraint in these in vitro models does not match the slowly evolving loss of prestrain that that accompanies non-traumatic disc degeneration, where nucleus pulposus depressurization can occur over many years. However, as noted above, these findings are consistent with reports from other soft tissues (i.e., tendon), where the acute release of boundary constraints or loss of tension results in an apoptotic response[25,26].

Contractility Mediates the Apoptotic Response upon Acute loss of Prestrain

A change in boundary condition alters tensional homeostasis[25] in cells, and their subsequent biologic response is to attempt to re-establish a balance between internal stresses and the microenvironment. In tendon, the increase in apoptotic events following acute rupture has

been ascribed to TGF-β signaling[26]. Interestingly, TGF-β signaling is intricately tied to contractility associated pathways, such as RhoA[30,31], and blocking TGF-β signaling attenuated the apoptotic response in previous studies. Given this, we hypothesized that cells experiencing an acute change in tensional homeostasis increase signaling associated with contractility, and that this ultimately exceeds the capacity of these cells for mechano-adaptation, ultimately instigating an apoptotic response. To test this hypothesis, we determined whether abrogation of contractility, using the ROCK inhibitor Y27632 and a clinically relevant ROCK inhibitor Fasudil[32-34], could attenuate this response. To determine the extent that these small molecule inhibitors reduce AF cell contractility, traction force microscopy of AF cells on 2D polyacrylamide substrates[21] was conducted and showed that both factors (at 10 μM) reduced the total contractile force of single AF cells by over 50% (Fig 6kl). When these factors were applied in the context of a release of prestrain, both attenuated the apoptotic response (Fig 6m-q). This finding supports that the notion that loss of tensional homeostasis, and the exuberant contractility that follows, is a driving factor in cellular response to altered boundary conditions. Such an insult leads to the death of a portion of the endogenous population and the emergence of a myofibroblastic population of cells survive this acute transition, and this promotes the fibrotic remodeling of the tissue.

Outlook

This work assessed the response of endogenous fibrous tissue cells to altered boundary constraints and the loss of residual strains in native tissue and in a biomaterial analogue. We discovered that, at the short time scale, loss of tension triggered an apoptotic response. With time, the remaining cell population re-initiated surveillance of this disorganized environment, and ultimately transitioned towards an activated myofibroblast-like phenotype. This phenotypic switch of cells within AF supports the progressive fibrotic remodeling seen after injury. To more precisely define how this altered fibrous environment directs such a phenotypic switch, we engineered a scaffold system that mimicked the time-evolving residual strains of injured tissue. Results using in vitro systems show that strain-mediated fiber topography can impact this mechanobiologic response. Disorganized fiber environments with slack and/or tortuous fibers tend to promote YAP/TAZ localization in the cytosol[35]. Conversely, straight fibers that are disorganized encourage nuclear localization of YAP/TAZ, along with cell spreading[36]. Here, we confirm such findings and further show that conditions with both high fiber alignment and pre-stress (reducing fiber tortuosity) promote a highly elongated cell morphology (tracking along a single or few fibers), which results in lower focal adhesion area and, consequently, lower nuclear YAP/TAZ. When the microenvironment was rapidly transitioned (by releasing prestrain), the emergent disorder drove cells to adopt a more random alignment and morphology, with increased nuclear YAP/TAZ localization, larger focal adhesions, and myofibroblast-like phenotypes closely mirroring that of native tissue.

While this study sought to decouple the effects of altered boundary constraints from the complex in vivo environment, it should be noted that there are a multitude of other factors that can mediate or tune the mechanosensing responses reported here. Inflammatory signaling can alter the mechanotransductive responses of annulus fibrosus[37-39]. Additionally, release of boundary constraints in tendon has been associated with release of TGFβ [26], and

this has been connected to apoptosis[26] and myofibroblast differentiation[18]. In the context of disc degeneration, while herniation is not always accompanied by inflammatory processes[40], injury and degeneration that are accompanied by inflammatory responses could exacerbate the mechanobiologic responses associated with the acute loss of pre-strain.

In all tissues, and particularly in fibrous tissues that have fixed boundaries, cells remodel the matrix to achieve a homeostatic set point, a so-called 'tensional homeostasis'[41-43]. In the AF and in AF-analogues that were prestrained, we determined that cells are relatively quiescent in a mechanobiologic sense. When pre-strain was increased acutely, we observed a productive mechanobiologic response, where cells increased their rate of calcium signaling to recover a tensional homeostasis. Conversely, when prestrain was acutely released, cells within the native tissue and biomaterial analogues were predisposed to an apoptotic response. In this context, re-engagement with a looser, disordered environment overwhelms the ability of cells to re-establish a productive equilibrium. While in some portion of the population, this triggered an apoptotic response, other cells developed a high stress, myofibroblastic phenotype to overcome the loss of prestress, as has been observed in severed tendon[42]. The acute response to loss of strain could be attenuated by blocking contractility pathways with the Rho pathway inhibitor Fasudil, which is clinically approved in several countries. These data support that contractility is a viable target for inhibition immediately following soft tissue injury (Fig 7). Blocking the early apoptotic/fibrotic cascade, coupled with surgical intervention to reestablish proper boundary constraints (i.e., NP replacement via a biomaterial injection combined with re-establishing AF connectivity[44-48]) may effectively inhibit this aberrant mechanobiologic feedback loop that culminates in soft tissue degeneration. Taken together, these findings may have implications for the treatment of all connective tissues that are subject to a loss of boundary constraints and undergo fibrotic remodeling after injury.

Methods

Rabbit Puncture Model

For *ex vivo* puncture experiments, 3 NZW rabbit spines were obtained from Sierra for Medical Science within 24 hours of sacrifice. From these, six motion segments (i.e., bone-disc-bone units, L2/L3 and L3/L4, n = 3 per group) were isolated and placed in a chemically-defined medium (CM) containing 1X penicillin/streptomycin/fungizone, 50 μg/mL ascorbate-2-phosphate, 40 μg/mL L-proline, 0.1 mM dexamethasone, and 100 μg/mL sodium pyruvate in high glucose DMEM for 1 hour. Following this equilibration, three discs were subjected to puncture of the anterior AF with a 16-gauge needle, to a depth of 5 mm (Fig 5a). The three remaining discs served as non-puncture controls. Following puncture, discs were cultured in CM for 24 hours prior to fixation for 1 week in 10% neutral buffered formalin and decalcification for 1 week in Formical. Samples were then processed into paraffin and sectioned for histological analysis.

For *in vivo* experiments, a total of nine NZW rabbits (~3kg) underwent puncture surgery (Charles River). Using an antero-lateral approach, the anterior portion of the AF was exposed under anesthesia. In a similar manner to the above, four motion segments were punctured per animal, with disc level confirmed via intraoperative x-ray (Fig 1a). Following

surgery, rabbits resumed normal cage activity and were monitored through a 2, 4, and 8-week post-surgical period. Following sacrifice, all L3/L4 motion segments (n = 3 per time point) were fixed and decalcified as above, prior to processing for histology. Additional punctured motion segments (L4/L5, L5/L6, and L6/L7) were allocated for mechanical analysis and for other unrelated studies. For mechanical analysis, samples were extracted, cleaned, cleared of posterior spinal elements, and frozen at −20C in PBS-soaked gauze prior to testing (n = 3 acute, 4 four and eight week, and 5 control and two week motion segments per group for mechanics).

Second Harmonic Generation Imaging and Quantification

Collagen organization was assessed via SHG imaging using an upright Nikon A1R multiphoton microscope. The system was equipped with a 16X water immersion objective with a 3 mm working distance. SHG imaging was conducted using a tunable wavelength laser set to 880 nm excitation. Both intact disc and slide mounted AF sections were viewed under the laser in the configuration depicted (Fig 5a). In each case, the focal plane for analysis was located ~200 μm into the anterior AF, as determined either by actuation of the z-stage for intact discs or via serial sectioning for slide-mounted samples. For each sample, z-stacks were obtained with 0.5 to 0.9 μm thick slices over a depth of 20 μm for intact discs or over the thickness for the 10 μm thick slide-mounted samples. For processing, z-stacks were imported into ImageJ and projected into an average intensity projection. This projection was then analyzed for fiber organization based on the FFT components using the directionality plugin for 90 bins over 180°. This raw data was imported into a custom excel file that fit the fiber angle distribution, f, by minimizing root-mean-square error to a Gaussian curve given by:

$$f(x) = a\, e^{-(x-b)^2/2c^2} \qquad \text{(equation 1)}$$

Where, a, b, and c are fitting parameters, and x is the fiber angle. The standard deviation of the fiber angle distribution, c, is reported as the angular spread, a measure of order/disorder of fiber distribution.

Electrospun Scaffold Preparation and Seeding

Electrospun poly(ε-caprolactone) (PCL) scaffolds were prepared as previously described[19,20,49]. Briefly, a 14% w/v solution of PCL in 1:1 tetrahydrofuran and dimethylformamide was loaded into a 10 mL syringe and extruded through a spinneret charged to 14 kV (1 kV/cm effective gradient to ground) and collected on a rotating, grouned mandrel. Spinning was conducted at room temperature in a humidty controlled room to 35% relative humidity. Both aligned and nonaligned scaffolds were prepared by tuning mandrel surface velocity (i.e., 14 m/s for aligned, 2.3 m/s for nonaligned). The fibers of the scaffold were measured as 200 nm (mode) for both aligned and nonaligned cases, and in the hydrated state PCL, accounted for ~9% of the scaffold weight (SFig 4). These electrospun mats were cut into 10 mm x 40 mm strips with the long axis corresponding to the prevailing fiber direction. To visualize fiber morphology and organization scaffolds were

mounted into the custom tensioning device depicted in figure 3a and placed in an environmental scanning electron microscope (ESEM, FEI Quanta 600 FEG Mark II). Fiber angle distributions were determined from ESEM images as described for the SHG analysis above, based on both baseline alignement (aligned vs nonaligned) and amount of applied axial strain (0% to 9%, in 3% increments).

Scaffolds for cell seeding were sterilized and rehydrated in 30 minute steps of progressively weaker ethanol (100%, 70%, 50%, and 30%) followed by 2 × 30 minute washes in sterile PBS. Scaffolds were incubated in fibronectin (20 μg/mL) overnight at 37°C. Cells were obtained from adult bovine caudal discs from 5 different animals, but not pooled. To isolate cells, discs were extracted from the caudal spine, separated from the vertebral bodies and the outer 2/3rd of the AF was isolated and minced. Special care was taken to remove any vascularized tissue at the disc periphery and the inner AF to mitigate cell heterogeneity. Following overnight isolation in collagenase, cells were plated and expanded through passage 0 in basal media (high glucose DMEM with 1X penicillin/streptomycin/fungizone and 10% fetal bovine serum) prior to cryopreservation. Once thawed, cells were used at passage 1 only, in order to minimize any effects the stiff environment of tissue culture polystyrene instills in the cells[12]. After passage 1 expansion in basal medium, cells were seeded by drop seeding on a 10 mm x 25 mm area of the PCL scaffolds at 5,000 (for single cell analyses: orientation, morphology, YAP/TAZ, paxillin) or at 25,000 cells per scaffold (for population-based analyses: αSMA incorporation, strain transfer, calcium signaling, caspase activation). Cells were then cultured at 37°C for 24 or 48 hours in CM under normoxic conditions and 5% CO2. Following culture, cells and scaffolds were fixed with 4% paraformaldehyde within their individual tensioning clamps (free swelling controls were also clamped, but no strain was applied) and these samples were maintained in their prestrained states through imaging.

Microcontact Printing

Microcontact printed substrates were fabricated as previously described[50]. Briefly, silicone substrates were fabricated using standard protocols with moduli ~100 kPa. The membranes were coated with fibronectin (50 ug/mL) and the PDMS stamps made by soft lithography was activated with UV/ozone. Fibronectin line patterns were generated by the stamp off method[50]. The membranes were then incubated in 0.2 mg/mL Pluronic F-127 for 30 minutes to passivate the remaining surface. Following fabrication, bovine AF cells were seeded for 24 hours prior to fixation with 4% paraformadehyde. Following similar permeabilization, staining, and imaging protocols as above, cells on both patterned and non-patterned substrates were assessed for cell and nuclear morphology as well as nuclear/cytoplasmic YAP/TAZ localization.

Immunofluoescent Staining, Imaging, and Analysis

Slide-mounted AF sections, cells on electrospun scaffolds, and cells on 2D substrates were all assessed via immunofluorescent staining. For slide-mounted AF sections, 10 μm paraffin embedded sections were cleared with Citrasolv and rehydrated in steps of progressively weaker ethanol, followed by washes with tris-buffered saline (TBS). Blocking was conducted with a commercial blocking reagent (Millipore product #20783) followed by

primary antibody incubation overnight at 4°C (rabbit polyclonal active caspase 3, Abcam antibody ab49822 1:500; alpha smooth muscle actin, Millipore Sigma antibody a2547 1:400). Following overnight incubation, samples were washed in TBS + 0.2% Tween-20 twice followed by secondary antibody incubation (goat anti-rabbit IgG or goat anti-mouse IgG at 1:200 in PBS supplemented with 1% bovine serum albumin). Following washes, slides were mounted with DAPI gold anti-fade prior to imaging on the Nikon A1R multiphoton microscope. For both caspase and αSMA, n = 3 discs were analyzed per group with at least 3 regions analyzed per disc. Both SHG and confocal fluorescence were captured for each of the three ROIs and are presented as the average intensity projection for SHG and the maximum intensity projection for the confocal fluorescence for caspase/αSMA and DAPI. For both analyses, imaging settings were held consistent (laser power: 3%, gain: 14, offset: 0).

Cells on 2D substrates and scaffolds were stained for YAP/TAZ (mouse anti-YAP/TAZ, 1:200), paxillin (mouse anti-paxillin 1:500), active caspase 3 (rabbit anti-caspase 1:500), and aSMA (mouse anti-aSMA, 1:400) using indirect immunofluorescence. Briefly, cells were fixed in 4% paraformaldahyde for 18 minutes prior to permeabilization in 0.5% Triton X-100 for 10 minutes. For paxillin staining, simultaneous permeabilization and fixation was conducted in 2% paraformadehyde with 0.1 M 1,4-piperazinediethanesulfonic acid, 1 mM EGTA, 1 mM magnerisum sulfate, 4% w/v poly(ethylene glycol), and 1% triton X-100 for 10 minutes at 37°C. Blocking was conducted using 1% bovine serum albumin during both the primary and secondary antibody incubations. Primary antibodies were applied at 4°C overnight. Secondary antibodies were applied for 1 hour (AlexaFluor 488, goat anti-mouse or goat anti-rabbit at 1:200 dilution) along with AlexaFluor 546 phalloidin (1:1000). Cell and nuclear aspect ratios were determined from cell and nuclear outlines that were fit to an ellipse using standard ImageJ analysis.

Functional Non-canonical Amino Acid Tagging (FUNCAT)

Nascent matrix deposition of annulus fibrosus cells on PCL scaffolds was assessed through FUNCAT staining[22]. Briefly, cell culture media (DMEM) without l-methionine was supplemented with the methionine analog, L-Azidohomoalanine (AHA), at 100 μM. Scaffolds were seeded with 5,000 cells per scaffold and cultured for 48 hours. Following culture, scaffolds were stained with the click chemistry fluorophore AFDye 488 DBCO (1:167 in PBS with 1% BSA) that labels azides in a copper-free reaction. Following 40 min of staining at 37°C, scaffolds were fixed for 18 minutes in 4% PFA prior to staining with AlexaFluor 546 phalloidin (1:1000) and Hoechst (1:10,000). Imaging was conducted on a confocal microscope as described above. Image analysis was conducted in ImageJ (SFig 10). Briefly, a sum slices projection was analyzed for local fiber organization and cell area from the blue and red channels, respectively. The nascent matrix deposition area was calculated from thresholded images and the deposition area was calculated as the area that was AHA+ minus the cell area. This metric of matrix deposition area was correlated with the local fiber organization.

Analysis of Calcium Transients

Cells seeded on scaffolds were assessed for spontaneous calcium signaling as previously described[28,49]. Following 24 hours of culture on scaffolds, samples were incubated in CM supplemented with 16 ug/mL Cal520-AM for 1 hour and Hoechst (1 μg/mL) to identify nuclei. Scaffolds were mounted on an inverted confocal microscope while in the clamps described above and denoted in Fig 2a. Clamps and scaffolds were bathed in cultured medium throughout testing. Samples were imaged at 0.25 Hz using a 488 laser for 10 minutes. Scaffolds were imaged both prior to and following stretch (4%−9%) or release (9% −4%). Following imaging, cells were identified and outlined based on the average intensity projection of all video frames with 25 cells identified per video (i.e., 25 per scaffold). For each cell, the Cal520-AM fluorescence intensity was collected as a function of time, and differentiated to obtain the time rate of change of fluorescent intensity, dI/d(t). The standard deviation of dI/d(t) over 10 minutes was calculated for each cell, and responding cells were identified as those that had calcium peaks indicated by dI/d(t) reaching levels that were 3 standard deviations above the mean dI/d(t) over the time course, using a custom Microsoft Excel template (SFig 13).

Traction Force Microscopy

Cells seeded on 2D polyacrylamide gels were assessed via traction force microscopy as previously described[21]. Briefly, 15 kPa polyacrylamide gels were fabricated containing 1% v/v FluoSpheres™ (0.2 μm diameter, red fluorescent, 2% solids) added prior to polymerization. Gels were coated with 20 μg/mL fibronectin for 1 hour prior to seeding with bovine AF cells. Gels were cultured 24 hours prior to analysis. 30 minutes prior to analysis Y27632 (10 μM) or Fasudil (10 μM) was added to the media with 1% bovine serum albumin to determine the effects of ROCK inhibition. Cell images were acquired prior to and following lysis with 10% sodium dodecyl sulfate. Both phase contrast (cell outline) and fluorescent channels (bead location) were collected for each cell. Analysis was conducted using the TFM plugin for ImageJ using the FTTC method as previously described[21]. Briefly, the displacement gradient field was calculated based on before and after images of the fluorescent beads. Phase contrast was used to determine the cell boundary and the total force (i.e., traction stress integrated over cell area) was reported for individual cells.

Statistical Analyses

Data and statistical analyses were conducted using Microsoft Excel, ImageJ, Matlab, and Prism as indicated above. For rabbit studies (mechanics, angular spread, IHC) either Student’s t-test (control versus puncture) or one-way ANOVA (control, 2 wk, 4 wk, 8 wk) were conducted with significance set at $p < 0.05$ and one- or two-tailed as appropriate. All analyses based on single cell measurements (shape, size, YAP/TAZ, focal adhesion area, local angular spread, traction force) were conducted using a Kruskal-Wallis test with Dunn’s test for multiple comparisons, as not all data were determined to be normally distributed. Additionally, outliers were identified using a Grubb’s test and removed from further analyses. Statistical analyses based on scaffold averages (αSMA and apoptosis) were conducted using the Friedman test with pairing within each independent experiment.

Correlations were conducted using a Pearson correlation coefficient. P-values are denoted within the figures.

Ethical Approval

The University of Pennsylvania Institutional Animal Care and Use Committee approved the live-animal portion of this study.

Supplementary Material

Refer to Web version on PubMed Central for supplementary material.

Acknowledgements

This study was supported by National Institutes of Health grants F32 AR072478, R01 EB02425, T32 AR053461, and P30 AR050950, the Department of Veteran's Affairs through grant I01 RX002274 and IK1 RX002445, and the Ministry of Science and Technology, Taiwan grants MOST107–2918-I-002–024, MOST107–2221-E-002–071-MY2 and National Health Research Institute NHRI-EX107–10411EI. Additional support was provided by the National Science Foundation via the NSF Science and Technology Center for Engineering Mechanobiology (CMMI-1548571). The authors would also like to thank Devon Mason and Joel Boerkel for assistance with traction force microscopy and Claudia Loebel and Jason Burdick for assistance with FUNCAT labeling of nascent matrix.

References

1. Adams MA & Roughley PJ What is Intervertebral Disc Degeneration, and What Causes It? Spine (Phila. Pa. 1976). 31, 2151–2161 (2006). [PubMed: 16915105]
2. Deyo RA, Mirza SK & Martin BI Back Pain Prevalence and Visit Rates. Spine (Phila. Pa. 1976). 31, 2724–2727 (2006). [PubMed: 17077742]
3. Lotz JC & Ulrich JA Innervation, Inflammation, and Hypermobility May Characterize Pathologic Disc Degeneration: Review of Animal Model Data. J. Bone Jt. Surg 88, (2006).
4. Urban JPG, Roberts S & Ralphs JR The Nucleus of the Intervertebral Disc from Development to Degeneration. Am. Zool 40, (2000).
5. Bonnevie ED & Mauck RL Physiology and Engineering of the Graded Interfaces of Musculoskeletal Junctions. Annu. Rev. Biomed. Eng 20, 403–429 (2018). [PubMed: 29641907]
6. Urban JP & Maroudas A Swelling of the intervertebral disc in vitro. Connect. Tissue Res 9, 1–10 (1981). [PubMed: 6456121]
7. Guehring T et al. Intradiscal pressure measurements in normal discs, compressed discs and compressed discs treated with axial posterior disc distraction: an experimental study on the rabbit lumbar spine model. Eur. Spine J 15, 597–604 (2006). [PubMed: 16133080]
8. Michalek AJ, Gardner-Morse MG & Iatridis JC Large residual strains are present in the intervertebral disc annulus fibrosus in the unloaded state. J. Biomech 45, 1227–1231 (2012). [PubMed: 22342138]
9. Plotnikov SV, Pasapera AM, Sabass B & Waterman CM Force Fluctuations within Focal Adhesions Mediate ECM-Rigidity Sensing to Guide Directed Cell Migration. Cell 151, 1513–1527 (2012). [PubMed: 23260139]
10. Dupont S et al. Role of YAP/TAZ in mechanotransduction. Nature 474, 179–183 (2011). [PubMed: 21654799]
11. Engler AJ, Sen S, Sweeney HL & Discher DE Matrix Elasticity Directs Stem Cell Lineage Specification. Cell 126, 677–689 (2006). [PubMed: 16923388]
12. Li CX et al. MicroRNA-21 preserves the fibrotic mechanical memory of mesenchymal stem cells. Nat. Mater 16, 379–389 (2017). [PubMed: 27798620]
13. Iatridis JC et al. Degeneration affects the anisotropic and nonlinear behaviors of human anulus fibrosus in compression. J. Biomech 31, 535–544 (1998). [PubMed: 9755038]

14. Masuda K et al. A novel rabbit model of mild, reproducible disc degeneration by an anulus needle puncture: correlation between the degree of disc injury and radiological and histological appearances of disc degeneration. Spine (Phila. Pa. 1976). 30, 5–14 (2005). [PubMed: 15626974]
15. Martin JT et al. Needle puncture injury causes acute and long-term mechanical deficiency in a mouse model of intervertebral disc degeneration. J. Orthop. Res 31, 1276–1282 (2013). [PubMed: 23553925]
16. Sivaguru M et al. Quantitative analysis of collagen fiber organization in injured tendons using Fourier transform-second harmonic generation imaging. Opt. Express 18, 24983 (2010). [PubMed: 21164843]
17. Tomasek JJ, Gabbiani G, Hinz B, Chaponnier C & Brown RA Myofibroblasts and mechano-regulation of connective tissue remodelling. Nat. Rev. Mol. Cell Biol 3, 349–363 (2002). [PubMed: 11988769]
18. Hinz B et al. The Myofibroblast: One Function, Multiple Origins. Am. J. Pathol 170, 1807–1816 (2007). [PubMed: 17525249]
19. Li W-J, Mauck RL, Cooper JA, Yuan X & Tuan RS Engineering controllable anisotropy in electrospun biodegradable nanofibrous scaffolds for musculoskeletal tissue engineering. J. Biomech 40, 1686–1693 (2007). [PubMed: 17056048]
20. Driscoll TP, Cosgrove BD, Heo S-J, Shurden ZE & Mauck RL Cytoskeletal to Nuclear Strain Transfer Regulates YAP Signaling in Mesenchymal Stem Cells. Biophys. J 108, 2783–2793 (2015). [PubMed: 26083918]
21. Cosgrove BD et al. N-cadherin adhesive interactions modulate matrix mechanosensing and fate commitment of mesenchymal stem cells. Nat. Mater 15, 1297–1306 (2016). [PubMed: 27525568]
22. McLeod CM & Mauck RL High fidelity visualization of cell-to-cell variation and temporal dynamics in nascent extracellular matrix formation. Sci. Rep 6, 38852 (2016). [PubMed: 27941914]
23. Loebel C, Mauck RL, Burdick J Local nascent protein deposition and remodeling guide mesenchymal stromal cell mechanosensing and fate in three-dimensional hydrogels. Nat. Mater in press, (2019).
24. Gardner-Morse MG & Stokes IA Physiological axial compressive preloads increase motion segment stiffness, linearity and hysteresis in all six degrees of freedom for small displacements about the neutral posture. J. Orthop. Res 21, 547–552 (2003). [PubMed: 12706030]
25. Egerbacher M, Arnoczky SP, Caballero O, Lavagnino M & Gardner KL Loss of Homeostatic Tension Induces Apoptosis in Tendon Cells: An In Vitro Study. Clin. Orthop. Relat. Res 466, 1562–1568 (2008). [PubMed: 18459026]
26. Maeda T et al. Conversion of Mechanical Force into TGF-β-Mediated Biochemical Signals. Curr. Biol 21, 933–941 (2011). [PubMed: 21600772]
27. Han WM et al. Microstructural heterogeneity directs micromechanics and mechanobiology in native and engineered fibrocartilage. Nat. Mater advance on, (2016).
28. Han WM et al. Impact of cellular microenvironment and mechanical perturbation on calcium signalling in meniscus fibrochondrocytes. Eur. Cell. Mater 27, 321–31 (2014). [PubMed: 24908425]
29. Godbout C et al. The Mechanical Environment Modulates Intracellular Calcium Oscillation Activities of Myofibroblasts. PLoS One 8, e64560 (2013). [PubMed: 23691248]
30. Edlund S, Landström M, Heldin C-H & Aspenström P Transforming Growth Factor-β–induced Mobilization of Actin Cytoskeleton Requires Signaling by Small GTPases Cdc42 and RhoA. Mol. Biol. Cell 13, 902–914 (2002). [PubMed: 11907271]
31. Zhang YE Non-Smad pathways in TGF-β signaling. Cell Res. 19, 128–139 (2009). [PubMed: 19114990]
32. Bond JE et al. Wound contraction is attenuated by fasudil inhibition of Rho-associated kinase. Plast. Reconstr. Surg 128, 438e–450e (2011).
33. Masumoto A et al. Suppression of coronary artery spasm by the Rho-kinase inhibitor fasudil in patients with vasospastic angina. Circulation 105, 1545–7 (2002). [PubMed: 11927519]

34. Shibuya M, Hirai S, Seto M, Satoh S & Ohtomo E Effects of fasudil in acute ischemic stroke: Results of a prospective placebo-controlled double-blind trial. J. Neurol. Sci 238, 31–39 (2005). [PubMed: 16005902]
35. Wan S et al. FAK- and YAP/TAZ dependent mechanotransduction pathways are required for enhanced immunomodulatory properties of adipose-derived mesenchymal stem cells induced by aligned fibrous scaffolds. Biomaterials 171, 107–117 (2018). [PubMed: 29684675]
36. Eichholz KF & Hoey DA Mediating human stem cell behaviour via defined fibrous architectures by melt electrospinning writing. Acta Biomater. 75, 140–151 (2018). [PubMed: 29857129]
37. Fearing BV, Hernandez PA, Setton LA & Chahine NO Mechanotransduction and cell biomechanics of the intervertebral disc. JOR Spine 1, e1026 (2018). [PubMed: 30569032]
38. Likhitpanichkul M et al. Do mechanical strain and TNF-α interact to amplify pro-inflammatory cytokine production in human annulus fibrosus cells? J. Biomech. 49, 1214–20 (2016). [PubMed: 26924657]
39. Tisherman R et al. NF- B Signaling Pathway in Controlling Intervertebral Disk Cell Response to Inflammatory and Mechanical Stressors. Phys. Ther 96, 704–711 (2016). [PubMed: 26893504]
40. Cooper RG et al. Herniated intervertebral disc-associated periradicular fibrosis and vascular abnormalities occur without inflammatory cell infiltration. Spine (Phila. Pa. 1976). 20, 591–8 (1995). [PubMed: 7604329]
41. Arnoczky SP et al. Loss of Homeostatic Strain Alters Mechanostat “Set Point” of Tendon Cells In Vitro. Clin. Orthop. Relat. Res 466, 1583–1591 (2008). [PubMed: 18459031]
42. Gardner K, Lavagnino M, Egerbacher M & Arnoczky SP Re-establishment of cytoskeletal tensional homeostasis in lax tendons occurs through an actin-mediated cellular contraction of the extracellular matrix. J. Orthop. Res 30, 1695–1701 (2012). [PubMed: 22517354]
43. Lavagnino M & Arnoczky SP In vitro alterations in cytoskeletal tensional homeostasis control gene expression in tendon cells. J. Orthop. Res 23, 1211–1218 (2005). [PubMed: 15908162]
44. Borde B, Grunert P, Härtl R & Bonassar LJ Injectable, high-density collagen gels for annulus fibrosus repair: An *in vitro* rat tail model. J. Biomed. Mater. Res. Part A 103, 2571–2581 (2015).
45. Sloan SR et al. Initial investigation of individual and combined annulus fibrosus and nucleus pulposus repair ex vivo. Acta Biomater. 59, 192–199 (2017). [PubMed: 28669721]
46. Gullbrand SE et al. Translation of an injectable triple-interpenetrating-network hydrogel for intervertebral disc regeneration in a goat model. Acta Biomater. (2017). doi:10.1016/j.actbio.2017.07.025
47. Chang G, Kim HJ, Vunjak-Novakovic G, Kaplan DL & Kandel R Enhancing annulus fibrosus tissue formation in porous silk scaffolds. J. Biomed. Mater. Res. Part A 92A, 43–51 (2010).
48. Séguin CA, Grynpas MD, Pilliar RM, Waldman SD & Kandel RA Tissue Engineered Nucleus Pulposus Tissue Formed on a Porous Calcium Polyphosphate Substrate. Spine (Phila. Pa. 1976). 29, 1299–1306 (2004). [PubMed: 15187628]
49. Han WM et al. Microstructural heterogeneity directs micromechanics and mechanobiology in native and engineered fibrocartilage. Nat. Mater 15, 477–484 (2016). [PubMed: 26726994]
50. Desai RA, Rodriguez NM & Chen CS “Stamp-off” to Micropattern Sparse, Multicomponent Features. Methods Cell Biol. 119, 3–16 (2014). [PubMed: 24439276]

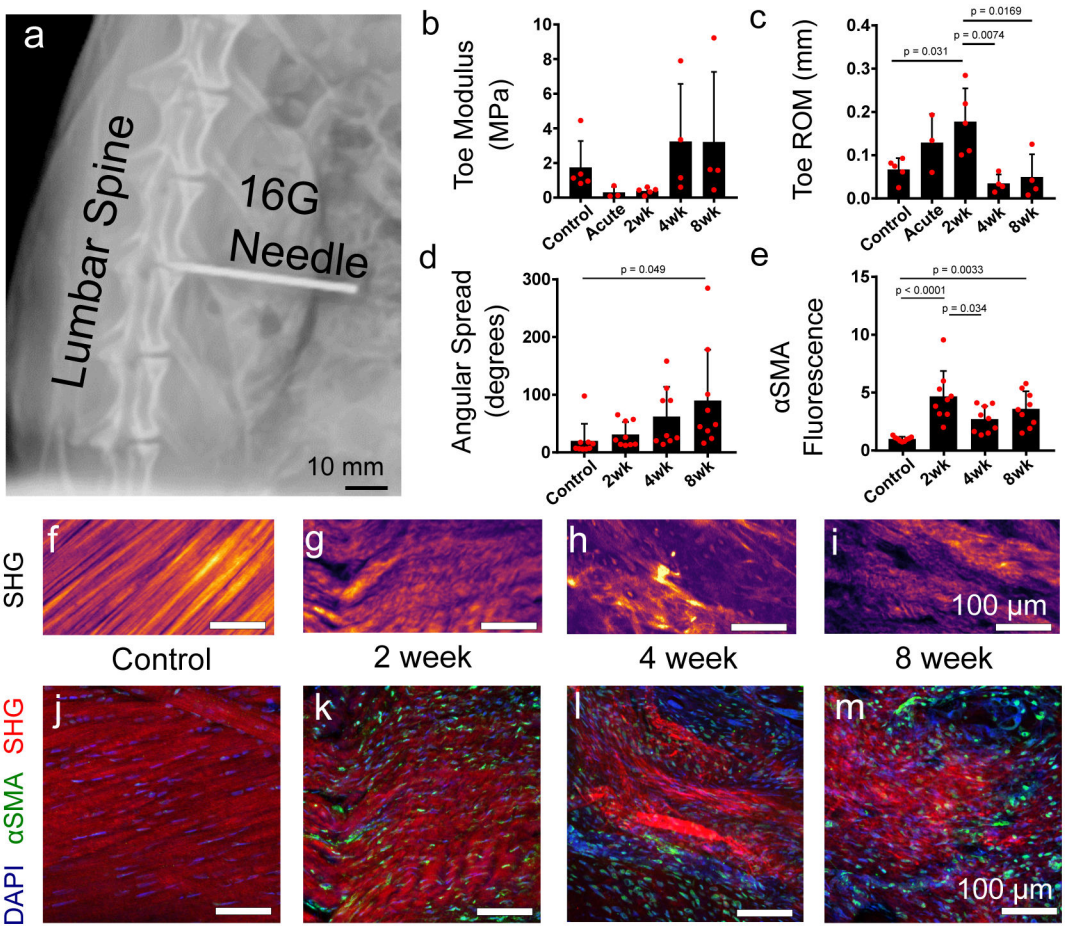

Fig. 1 |. *In vivo* disc puncture and release of residual strains alters mechanics and initiates aberrant remodeling of the disc.

(a) Intra-operative radiograph of AF puncture surgery performed in New Zealand White rabbits. Puncture resulted in acute and time-dependent mechanical changes to the whole disc, with altered range of motion (ROM, c) and toe-region modulus (b). (d, f-i) Second harmonic generation (SHG) imaging of the outer AF revealed a progressive loss of fiber organization and increasing angular spread (i.e., the standard deviation of the fiber angle distribution). Staining for alpha smooth muscle actin (αSMA) and all nuclei (DAPI, 4′,6-diamidino-2-phenylindole) showed an emergent pro-fibrotic phenotype as soon as 2 weeks following injury, which remained elevated through 8 weeks (e, j-m). One-way analysis of variance was used with Dunnett's post hoc for statistical analyses (n = 3 acute, 4 four and eight week, and 5 control and two week motion segments per group for mechanics, and n = 3 discs per group with 3 ROIs each for histologic analyses, bars denote mean and standard deviation).

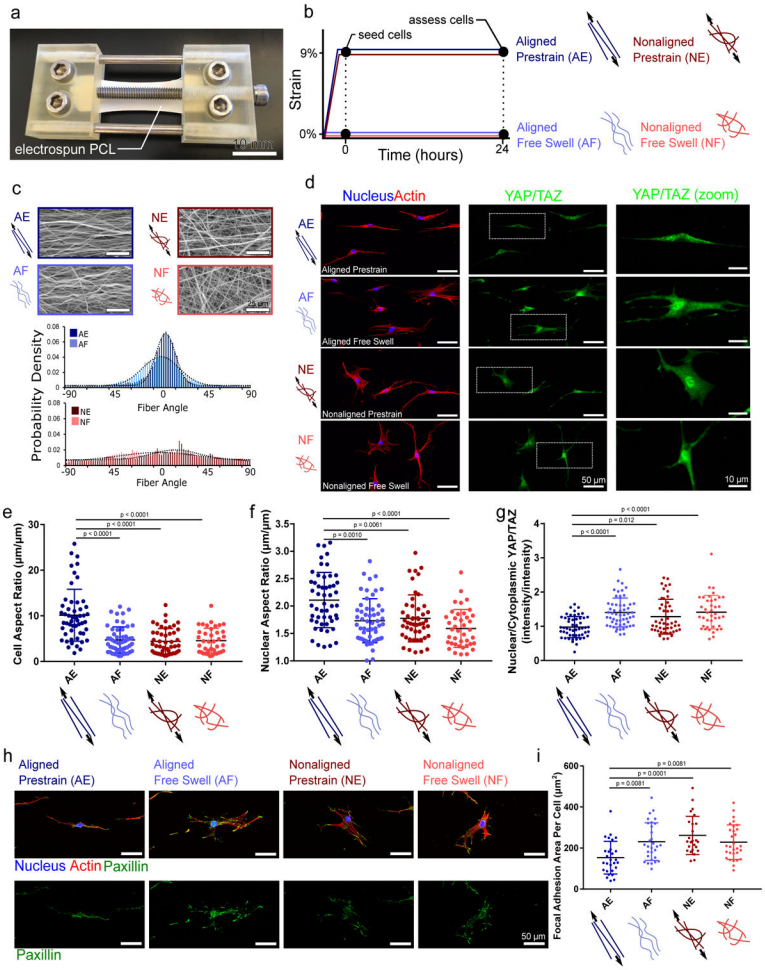

Fig. 2 l. Scaffold-based system to evaluate impact of prestrain in fibrous microenvironments.
(a) Scaffold tensioning clamps were used to (b) apply prestrain to electrospun scaffolds. (c) Stretching scaffolds in an environmental scanning electron microscope revealed strain-mediated fiber organization. (d) Bovine annulus fibrosus cells seeded onto scaffolds exhibited fiber alignment-modulated (e) cell (f) and nuclear morphology. (d,g) Prestrain in aligned scaffolds reduced nuclear YAP/TAZ and (h,i) resulted in lower focal adhesion area per cell. Kruskal-Wallis testing with Dunn's multiple comparisons post hoc were used to determine statistical significance on cells from at least 2 donors per group (e-g, n = 52 AE, 58 AF, 49 NE, and 41 NF cells per group; i, n = 28 AE, 30 AF, 25 NE, and 30 NF cells per group, bars denote mean and standard deviation).

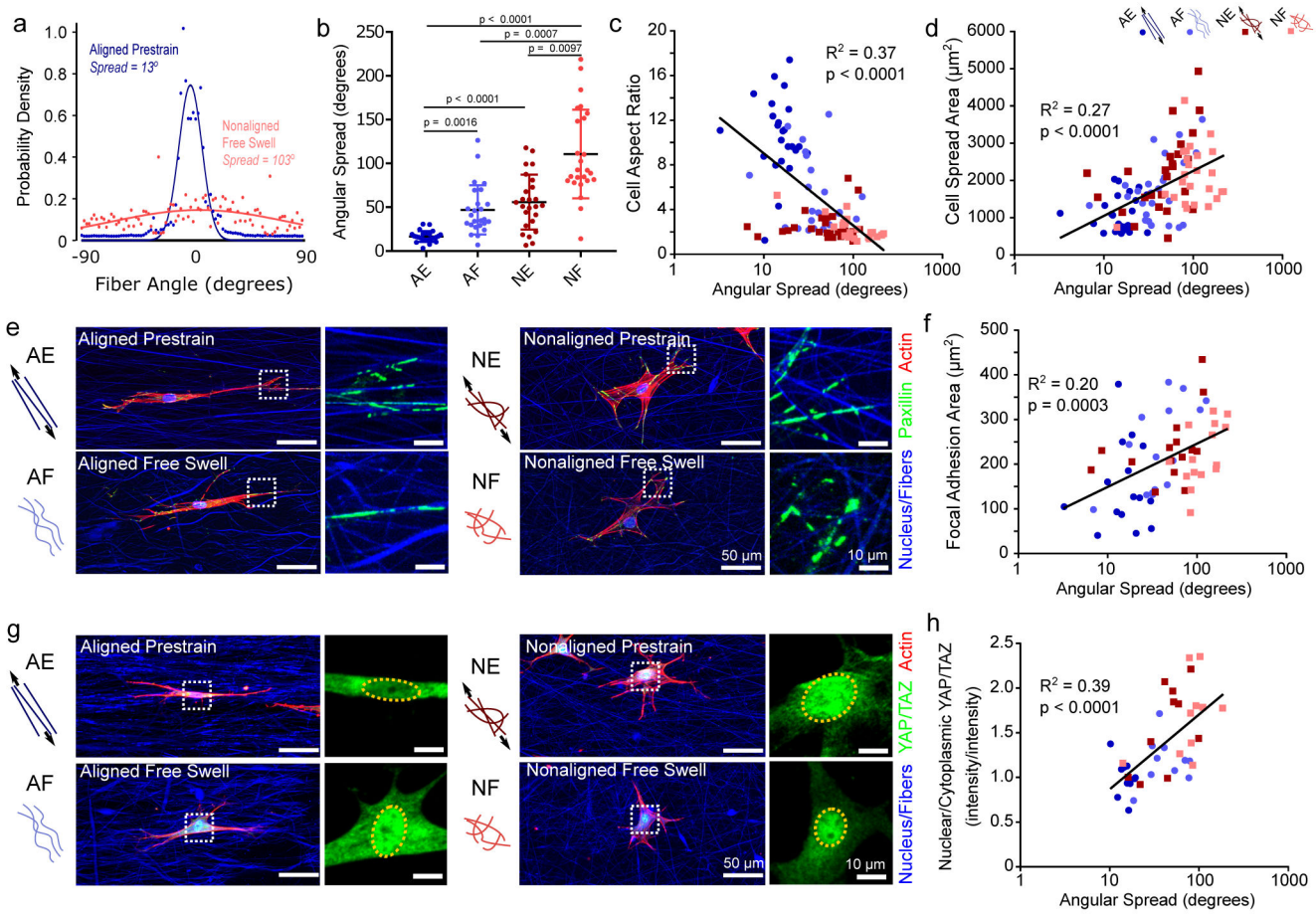

Fig. 3 |. Boundary conditions and fiber organization govern cell spreading and mechanosensation.

(a, b) Local fiber angle distributions to calculate angular spread revealed dependence on baseline and strain-mediated fiber organization. (c,d) Angular spread was predictive of both bovine annulus fibrosus cell shape (i.e. aspect ratio) and spread area. (e,f) Focal adhesions visualized via paxillin staining (green), along with fibers and nuclei (blue) and actin cytoskeleton (red), showed that focal adhesion area could be predicted by local fiber organization. (g,h) YAP/TAZ staining revealed that mechanosensation was predicted by local fiber organization, where more organized fiber environments resulted in lower nuclear YAP/TAZ nuclear localization. Dashed boxes denote zoom-in areas and dashed ellipses denote the nuclear outline. Statistical analyses were conducted using (b) Kruskal-Wallis testing with Dunn's multiple comparisons post hoc and (c,d,f,h) Pearson's correlation coefficient (b-d: n = 100 cells total from 5 scaffolds per group; e-f: n = 60 cells total from 3 scaffolds per group; g-h: n = 40 cells total from 2 scaffolds per group, bars denote mean and standard deviation).

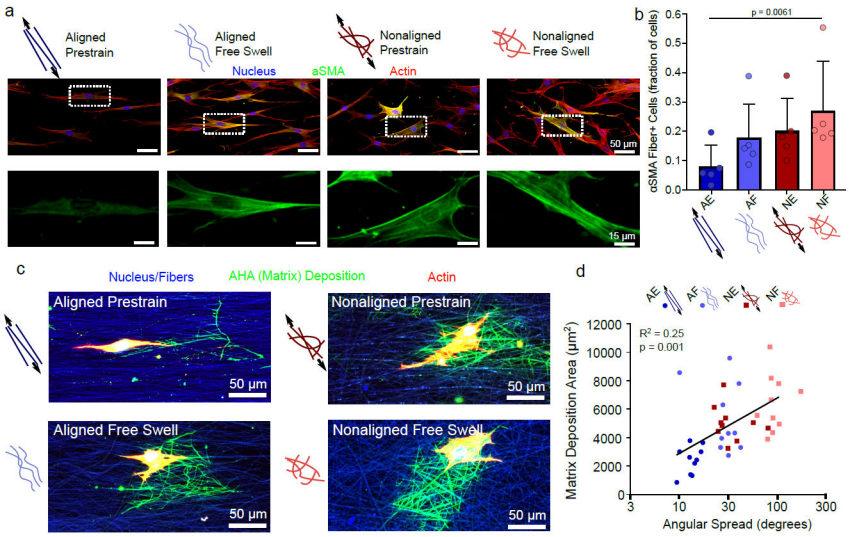

Fig. 4 |. Local fiber organization mediates AF cell phenotype and biosynthetic response.
(a) Staining for aSMA revealed a connection between fiber organization and the emergence of a myofibroblast-like phenotype in bovine annulus fibrosus cells. (b) Significantly more cells exhibited aSMA+ stress fibers in free swelling nonaligned scaffolds compared to aligned prestrained scaffolds. (c) FUNCAT staining revealed nascent matrix deposition with single cell resolution. (d) Angular spread predicted the biosynthetic response of AF cells, where more disorganized environments promoted more matrix deposition. Statistical significance was determined using (b) Friedman test with data paired by experimental set followed by Dunn's multiple comparisons post hoc and (d) Pearson's correlation coefficient (a,b: n = 5 scaffolds per group paired by donor/experiment, average of 94 cells analyzed per scaffold; c-d n = 40 cells from 1 donor, bars denote mean and standard deviation).

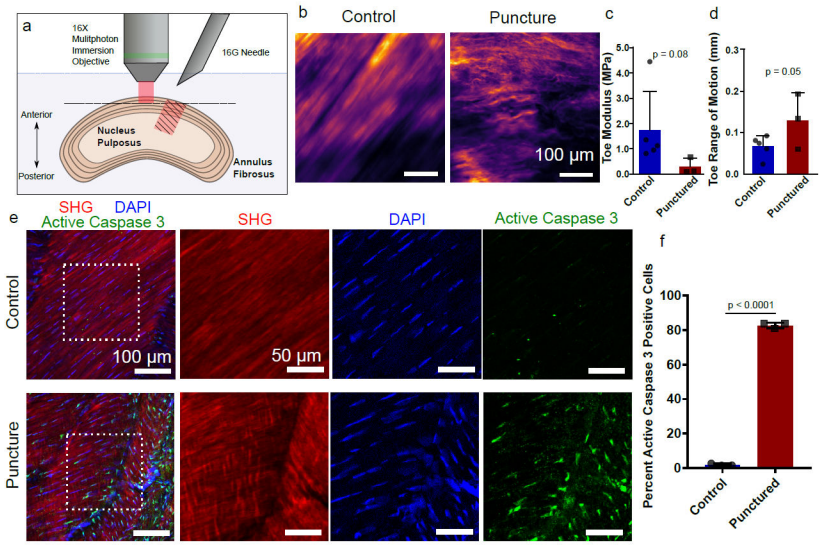

Fig. 5 |. *In vitro* disc puncture releases residual strain, altering fiber morphology, disc mechanics, and triggering apoptosis.

(a,b) Whole New Zealand White rabbit motion segments were mounted below a multiphoton objective and the AF was imaged prior to and following puncture with a 16-gauge needle via second harmonic generation (SHG) imaging for collagen content and organization. Dotted line denotes imaging plane 50 – 100 μm from the tissue surface, with the puncture region denoted by the red hashed area. (c,d) Acutely, puncture reduced whole disc stiffness and increased range of motion indicating improper actuation of the AF under axial loading. Statistical significance was determined using an unpaired one-tailed t-test (n = 3 acute and 5 control motion segments per group, SFig 1 for details). (e,f) Motion segments cultured for 24 hours following puncture showed an apoptotic response in endogenous AF cells. Statistical significance was determined using an unpaired two-tailed t-test (n = 3 discs per group, ~500 cells per disc, SFig 2 for details). Bars denote mean and standard deviation. Scale bars are 100 μm for merged images and 50 μm for split channels.

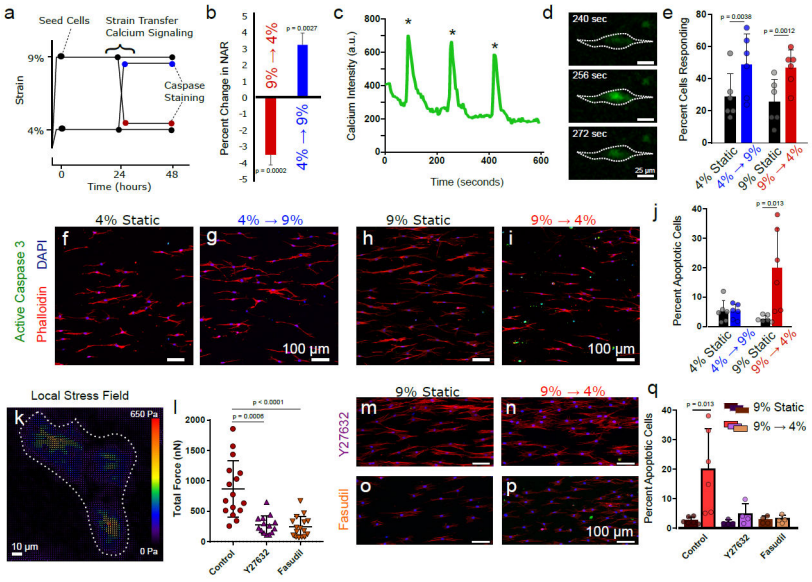

Fig. 6 | Cells respond differently to stretch and release of tension.

(a) Schematic of experiments to study the effects of altering boundary constraints in fibrous environments (i.e., stretch, blue symbols, or release of prestrain, red symbols). (b) Both stretch (4%→9%) and release (9%→4%) resulted in changes in nuclear aspect ratio revealing strain transfer from the scaffold to bovine annulus fibrosus cells (statistical significance was determine using an unpaired two-tailed t-test between static and stretch or release, n = 512 4% Static, 747 4%→9%, 845 9% Static, and 706 9%→4% cells per group from 3 scaffolds per group). Monitoring spontaneous calcium signaling (c, d) before and after altering the boundary constraints revealed a significant increase in the percentage of cells responding (e, statistical significance was determined using a paired two-tailed t-test, where scaffolds were paired by donor and experiment, n = 6 scaffolds per group, 25 cells per scaffold. A single cell's trace is shown for a 10-minute test following strain release with this cell outlined with a white dashed line. Release of prestrain (9%→4%) triggered apoptosis as assayed 24 hours after actuation, while stretch (4%→9%) did not, as evidenced by active caspase 3 staining (f-j; statistical significance was determined using an unpaired two-tailed t-test, n = 6 scaffolds per group from 3 donors). (k) Traction force microscopy showed (l) blocking the ROCK pathway with either Y27632 or Fasudil decreased AF cell contractility (statistical significance was determined using Kruskal-Wallis testing with Dunn's multiple comparisons post hoc, n = 16 control and n = 14 Y27632 and fasudil) and (m-q) attenuated the apoptotic response triggered by loss of prestrain (statistical significance was determined using an unpaired two-tailed t-test, n = 6 scaffolds for control and 4 for Y27632 and Fasudil per group where scaffolds represent independent samples). Bars denote mean and standard deviation.

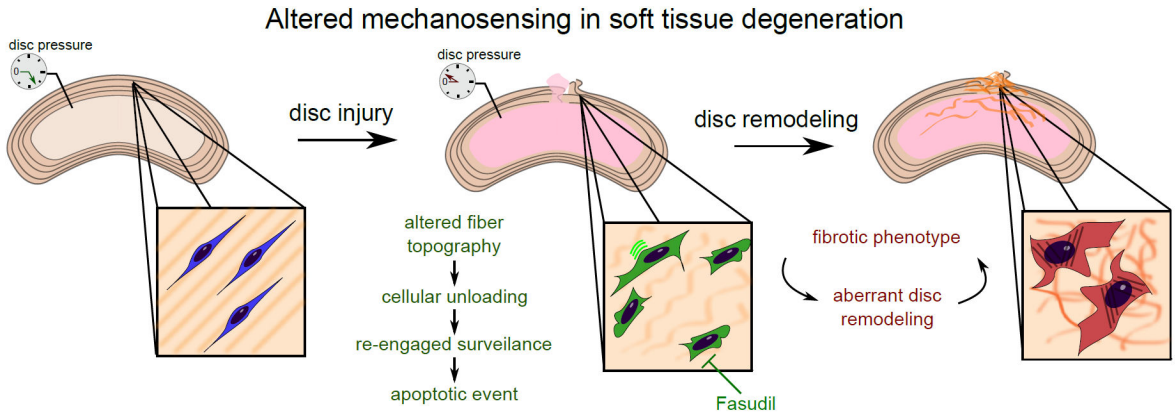

Fig. 7 |. Disc injury initiates altered mechanosensing leading to soft tissue degeneration.
Disc injury alters the boundary constraints of the AF and ensuing aberrant events can be blocked by inhibiting cellular contractility at the time of injury. Untreated, these acute changes result in a feedback loop that drives aberrant disc remodeling, where remodeling causes more disorganized ECM and disorganized ECM promotes a fibrotic phenotype. Together, this supports the importance of mechanobiologic cues that arise within highly aligned soft tissue environments after injury.